

## Density-functional approach to local-field effects in finite systems: Photoabsorption in the rare gases

A. Zangwill and Paul Soven

*Department of Physics and the Laboratory for Research on The Structure of Matter, University of Pennsylvania, Philadelphia, Pennsylvania 19174*

(Received 29 October 1979)

We present a formalism based on density-functional theory capable of describing polarization-type many-body effects influencing the photoresponse of small electronic systems. The self-consistent field approach we describe incorporates correlations into a local, effective single-particle potential which takes account of the time-dependent fields induced by an external radiation field. In this paper we present calculations of the static polarizabilities, total photoabsorption cross sections, and selected partial photoabsorption cross sections of the rare gases which yield results in good agreement with experiment. A study of the energy and spatial dependence of the local field leads to a clear physical picture of the dielectric properties of these systems.

### I. INTRODUCTION

In this paper, we demonstrate the applicability of the density-functional formalism to the accurate description of certain many-body effects which influence the photoabsorption spectra of the rare gases. We describe a self-consistent field procedure<sup>1</sup> which takes account of polarization phenomena<sup>2</sup> in these small electronic systems. Our calculations, based on simple, nonbasis set, numerical techniques, yield results for the atomic polarizability and photoabsorption cross section in good agreement with experiment. We focus particular attention on the effective, self-consistent, local field to which the electrons respond independently. All the electron correlation effects we consider are incorporated into this local field, taken to be the sum of the external field and those fields induced by perturbations of the electron charge density.<sup>3</sup> We gain insight into the nature of the dielectric response in these finite systems by a study of this position and frequency dependent field. The present work is confined to atoms and is meant to be exploratory in nature. Nonetheless, we feel that our approach should be well suited to the study of similar phenomena in more complex systems as well.

The phenomena under study fall generally into the category of electron correlation effects. The importance of these effects in many-electron systems has long been stressed.<sup>4-7</sup> For example, correlations are known to make a sizable contribution to the total energy and magnetic susceptibility of the infinite electron liquid.<sup>8</sup> Indeed, an entirely new mode (the plasmon) appears solely through collective effects. Quite generally, one finds a redistribution of a system's

spectral weight from that obtained when interactions between the electrons are neglected.

In systems with relatively few electrons, such as atoms and molecules, one continues to find important many-body effects. Again, correlations may affect ground-state properties considerably<sup>9</sup>; however, it is the excitation spectra which often most clearly reveal the influence of electron interactions. Double photoionization<sup>10</sup> and shake-up<sup>11</sup> are examples of processes with two electron-hole pairs in the final state which occur only through strong correlations. More subtle effects, such as oscillator strength redistribution, only become apparent with the failure of independent-particle calculations to describe the observed cross sections.<sup>12</sup> This failure has been the focus of much of the recent work in the field and is the issue we address here as well.

Considerable progress has been made in the past ten years toward incorporating polarization-type many-body effects into the calculation of atomic properties. The early work of Altick and Glassgold<sup>13</sup> has been extended and refined by several groups to the point where the random phase approximation with exchange (RPAE) provided a very successful description of atomic photoabsorption in most cases.<sup>14,15</sup> Similarly, good results have emerged from the extensive work by Kelly and co-workers with the many-body perturbation theory (MBPT).<sup>16</sup> A useful review of these methods placing them in the context of the early configuration-interaction (CI) approach is presented by Chang and Fano.<sup>17</sup> Finally, we mention the impressive results found with the so called *R*-matrix methods.<sup>18</sup> All the above calculations have produced photoabsorption cross sections for a variety of atoms in good accord with experiment. However, a crucial fea-

ture of all these techniques seems to be the cost paid in computational effort as the system complexity increases; the practical extension of these methods to even small molecules appears extremely difficult at present.

The formalism described in this paper includes correlation effects at the same level as much of the work mentioned in the previous paragraph. The essential advantage of our approach is the computational simplicity provided by the density-functional formalism (or more specifically the local approximation to it). In particular, certain infinite summations over the atomic spectrum may be performed exactly with a Green's function appropriate to the local, ground-state, effective potential. Furthermore, the time-dependent screening fields induced by the external field also are completely local, facilitating a conceptual, as well as computational, simplification not achieved with a Hartree-Fock-based calculation. We have chosen to test our procedure with the rare-gas atoms for three reasons: (1) there exists a wealth of experimental data, (2) a great many calculations already exist with which to compare our results, and (3) some simplicity in the formalism is achieved for closed-shell systems. The results indicate that the methods of local density-functional theory are quite appropriate for an accurate description of the photoabsorption process, at least in these systems.

The outline of the paper is as follows. In Sec. II we present the linear response theory of the atomic polarizability and photoabsorption cross section. Our application of density-functional techniques and the self-consistent field (SCF) method are then outlined. Some details of the calculation such as the construction of the atomic Green's function and the computation of partial cross sections are discussed in Sec. III. We present our results for the atomic polarizability and total cross section of the rare-gas atoms and the 3s partial cross section of argon in Sec. IV and interpret them in terms of the local field. We conclude with a brief summary.

## II. GENERAL FORMALISM

### A. Atomic polarizability and photoabsorption cross section

In this section we discuss the photoresponse of an isolated atom to an external electromagnetic field in terms of the frequency-dependent polarizability  $\alpha(\omega)$ . In the case where the wavelength of the radiation is large compared with atomic dimensions, the interaction Hamiltonian may be written as  $\mathcal{H}' = \int n(\vec{r}, t) \phi^{\text{ext}}(\vec{r}, \omega) e^{-i\omega t} d\vec{r}$ . In general, the external field will induce time-dependent perturbations in the electronic density. We de-

note the deviations from the unperturbed density distribution by  $\delta n(\vec{r}, t)$ . Since only the linear response is of interest, we may treat each Fourier component of this disturbance individually. The Fourier components are defined by

$$\delta n(\vec{r}, t) = \frac{1}{2\pi} \int_{-\infty}^{+\infty} \delta n(\vec{r}, t) e^{-i\omega t} d\omega. \quad (1)$$

The induced density and the external potential are related through a position- and frequency-dependent complex susceptibility,

$$\delta n(\vec{r}, \omega) = \int \chi(\vec{r}, \vec{r}'; \omega) \phi^{\text{ext}}(\vec{r}', \omega) d\vec{r}'. \quad (2)$$

Conventional first-order time-dependent perturbation theory<sup>19</sup> shows that  $\chi(\vec{r}, \vec{r}'; \omega)$  may be written as the time Fourier transform of a retarded density-density correlation function,

$$i\hbar\chi(\vec{r}, \vec{r}'; t - t') = \vartheta(t - t') \langle 0 | [\hat{n}(\vec{r}, t), \hat{n}(\vec{r}', t')] | 0 \rangle. \quad (3)$$

In this expression,  $|0\rangle$  is the exact many-particle ground state,  $\hat{n}(\vec{r}, t)$  the Heisenberg particle density operator, and  $\vartheta(t - t')$  the unit step function. Inserting a complete set of many-particle states  $|m\rangle$  and Fourier transforming, we obtain the spectral representation

$$\chi(\vec{r}, \vec{r}'; \omega) = \sum_m \frac{\langle 0 | \hat{n}(\vec{r}) | m \rangle \langle m | \hat{n}(\vec{r}') | 0 \rangle}{\hbar\omega - (E_m - E_0) + i\delta} - \frac{\langle 0 | \hat{n}(\vec{r}') | m \rangle \langle m | \hat{n}(\vec{r}) | 0 \rangle}{\hbar\omega + (E_m - E_0) + i\delta}, \quad (4)$$

where the  $E_m$  are the exact energy levels and  $\delta$  a positive infinitesimal. Complete knowledge of the wave functions and energies determines the induced density through Eqs. (2) and (4).

In the present case it is sufficient to set

$$\phi^{\text{ext}}(\vec{r}, \omega) = \frac{1}{2} e \mathcal{E}_0 z, \quad (5)$$

where  $\mathcal{E}_0$  is the magnitude of the external electric field and  $e$  is a positive quantity. The actual perturbation is  $\mathcal{H}' = e z \mathcal{E}_0 \cos \omega t$ . The frequency-dependent polarizability  $\alpha(\omega)$  is the ratio of the induced dipole moment to the external field strength:

$$\alpha(\omega) = - \frac{2e}{\mathcal{E}_0} \int z \delta n(\vec{r}, \omega) d\vec{r}, \quad (6)$$

$$\alpha(\omega) = -e^2 \int z \chi(\vec{r}, \vec{r}'; \omega) z' d\vec{r} d\vec{r}'. \quad (7)$$

An explicit expression for  $\alpha(\omega)$  is found by substituting Eq. (4) into Eq. (7) and using

$$\hat{n}(\vec{r}) = \sum_{i=1}^N \delta(\vec{r} - \vec{r}_i),$$

where  $N$  is the number of electrons in the atom. The result is

$$\alpha(\omega) = -e^2 \sum_m \left[ \frac{|\langle m | \hat{z} | 0 \rangle|^2}{\hbar\omega - (E_m - E_0) + i\delta} - \frac{|\langle m | \hat{z} | 0 \rangle|^2}{\hbar\omega + (E_m - E_0) + i\delta} \right], \quad (8)$$

where  $\hat{z} = \sum_i z_i$ . The imaginary part of this expression is proportional to the Golden Rule formula for the photoabsorption cross section,

$$\sigma(\omega) = 4\pi(\omega/c) \text{Im}\alpha(\omega), \quad (9)$$

and the static polarizability is found by setting  $\omega=0$  in Eq. (8),

$$\alpha(0) = -2e^2 \sum_m \frac{|\langle m | \hat{z} | 0 \rangle|^2}{E_0 - E_m}. \quad (10)$$

It will be useful subsequently if we review two properties of the zero-frequency polarizability. First, as may be readily verified, the photoabsorption cross section satisfies a sum rule,<sup>20</sup>

$$\int_0^\infty \frac{\sigma(\omega)}{\omega^2} d\omega = \frac{2\pi^2}{c} \alpha(0). \quad (11)$$

Second,  $\alpha(0)$  is a ground-state property of an atom in the presence of a static electric field. Indeed, it is well known<sup>21</sup> that the static polarizability follows directly from a second-order time-dependent perturbation-theory calculation of the total ground-state energy of an atom subject to the perturbation  $\mathcal{H}'$  with  $\omega=0$ :

$$E_{\text{total}} = E_0 - \frac{1}{2}\alpha(0)\mathcal{E}_0^2 + \dots \quad (12)$$

We stress that no such relationship exists for  $\alpha(\omega)$  for nonzero frequency.

### B. Independent-particle approximation

A first approximation to the photoresponse problem treats the atomic electrons as responding independently to the external field, Eq. (5). The many-particle wave function is constructed as a single Slater determinant of single-particle orbital eigenfunctions of an effective single-particle potential. In such a scheme, the photoabsorption cross section, Eq. (9) reduces to

$$\sigma(\omega) = 4\pi^2 \alpha \hbar\omega \sum_{i,j} f_i (1 - f_j) |\langle j | z | i \rangle|^2 \times \delta(\hbar\omega - \epsilon_j + \epsilon_i), \quad (13)$$

where the  $\epsilon_i$  are the single-particle energy eigenvalues,  $\alpha$  is the fine-structure constant, and the  $f_i$  are Fermi occupation factors. Note from this formula that the absorption occurs at photon energies equal to differences of single-particle energies with strength determined by matrix elements of the *external* field. Rather extensive calculations of atomic photoabsorption cross sections have been performed in an independent-

particle model of this type.<sup>22,23</sup> These studies show that the basic trends of the photoabsorption spectra for a variety of atoms are well reproduced; however, there exist considerable discrepancies between the computed magnitudes and the measured absolute cross sections. Hartree-Fock calculations<sup>24</sup> yield somewhat improved results although systematic deviations from the data remain. It is now clear that good agreement with experiment may often only be achieved by the inclusion of dielectric effects in cross-section calculations.<sup>25</sup> Our approach to this problem is largely based on the methods of the local-density-functional formalism; we therefore begin with a brief review of its essential features.

### C. The local-density approximation

The density-functional formalism<sup>26</sup> treats the particle density  $n(\vec{r})$  as the basic quantity in a theory of the ground-state properties of many-particle systems. In particular, the ground-state density in an atom is determined by simultaneous solution of the following equations:

$$[-(\hbar^2/2m)\nabla^2 + V_{\text{eff}}(\vec{r})]\varphi_i(\vec{r}) = \epsilon_i \varphi_i(\vec{r}), \quad (14)$$

$$V_{\text{eff}}(\vec{r}) = V_N(\vec{r}) + e^2 \int \frac{n(\vec{r}')}{|\vec{r} - \vec{r}'|} d\vec{r}' + \frac{\delta E_{\text{xc}}[n]}{\delta n(\vec{r})}, \quad (15)$$

$$n(\vec{r}) = \sum_{i=1}^N |\varphi_i(\vec{r})|^2. \quad (16)$$

$E_{\text{xc}}[n]$  is the (generally unknown) exchange-correlation energy functional and  $V_N(\vec{r})$  is the nuclear potential. The exchange-correlation potential is obtained by functional differentiation as indicated. If the exact functional were known, this procedure would yield the exact ground-state density. In practice, one tries to construct suitable approximations for  $E_{\text{xc}}[n]$ .

A commonly used approximation is the local-density approximation (LDA).<sup>27</sup> The total exchange-correlation energy is presumed to be

$$E_{\text{xc}}[n] = \int n(\vec{r}) \epsilon_{\text{xc}}[n(\vec{r})] d\vec{r}, \quad (17)$$

where  $\epsilon_{\text{xc}}$  is the exchange-correlation energy per particle for a homogeneous system with density  $n(\vec{r})$ . This is a tremendous simplification since it leads to a local exchange-correlation potential,

$$V_{\text{xc}}(\vec{r}) = \frac{\partial}{\partial n(\vec{r})} [n(\vec{r}) \epsilon_{\text{xc}}(n(\vec{r}))]. \quad (18)$$

The LDA equations [(14)–(16)] are then no more difficult to solve than the Hartree equations.

Extensive work<sup>28</sup> has shown that the ground-state properties of many systems are well described by the LDA.

It should be stressed that the quantities  $\varphi_i(\vec{r})$  and  $\epsilon_i$  which enter the LDA equations are merely auxiliary quantities in the calculation of the particle density. They have not been shown to have an independent physical meaning. Nonetheless, we treat them as representing wave functions and energy levels which characterize the ground state. Furthermore, we use the continuum orbitals generated by  $V_{\text{eff}}(\vec{r})$  as final states in the photoabsorption process.<sup>29</sup> Our aim is to determine whether such a procedure can lead to a sensible description of a phenomenon which crucially involves excited states of the system. In practice, we employ a parametrized expression for  $V_{\text{xc}}(\vec{r})$  taken from Ref. 7 (in Ry),

$$V_{\text{xc}}(\vec{r}) = -\frac{1.222}{r_s(\vec{r})} - 0.0666 \ln\left(1 + \frac{11.4}{r_s(\vec{r})}\right), \quad (19)$$

where  $\frac{4}{3}\pi r_s^3(\vec{r}) = n(\vec{r})^{-1}$ . The results of this section provide the material for an independent particle calculation.

#### D. The self-consistent-field procedure

If the electrons of the atom were truly non-interacting, the induced density in the presence of the external field would be

$$\delta n(\vec{r}, \omega) = \int \chi_0(\vec{r}, \vec{r}'; \omega) \phi^{\text{ext}}(\vec{r}', \omega) d\vec{r}'. \quad (20)$$

The subscript indicates that we form the independent-particle version of Eq. (4),

$$\chi_0(\vec{r}, \vec{r}'; \omega) = \sum_{i,j} (f_i - f_j) \times \frac{\varphi_i^*(\vec{r})\varphi_j(\vec{r})\varphi_j^*(\vec{r}')\varphi_i(\vec{r}')}{\hbar\omega - (\epsilon_j - \epsilon_i) + i\delta}, \quad (21)$$

using wave functions and energies obtained from the LDA calculation. The particle density represented by Eq. (20) reflects the response to the external field alone. However, as the electrons redistribute themselves through the atom, they interact with one another through the Coulomb interaction. That is, an individual electron experiences a field produced by its neighbors in addition to the external field.<sup>30</sup> This effect is represented in an average way by an induced Coulomb potential energy

$$\delta V_{\text{C}}(\vec{r}, \omega) = e^2 \int \frac{\delta n(\vec{r}', \omega)}{|\vec{r} - \vec{r}'|} d\vec{r}', \quad (22)$$

and an induced exchange-correlation potential energy

$$\delta V_{\text{xc}}(\vec{r}, \omega) = \frac{\partial V_{\text{xc}}}{\partial n} \Big|_{n=n(\vec{r})} \delta n(\vec{r}, \omega), \quad (23)$$

obtained by linearizing the LDA functional [Eq. (19)] around the ground-state density.<sup>31</sup> We define

$$\begin{aligned} \phi^{\text{ind}}(\vec{r}, \omega) &= \delta V_{\text{C}}(\vec{r}, \omega) + \delta V_{\text{xc}}(\vec{r}, \omega) \\ &= \int K(\vec{r}, \vec{r}') \delta n(\vec{r}', \omega) d\vec{r}', \end{aligned} \quad (24)$$

and require the electrons to respond independently to a new, local driving field. That is,

$$\begin{aligned} \delta n(\vec{r}, \omega) &= \int \chi_0(\vec{r}, \vec{r}'; \omega) [\phi^{\text{ext}}(\vec{r}', \omega) + \phi^{\text{ind}}(\vec{r}', \omega)] d\vec{r}' \\ &= \int \chi_0(\vec{r}, \vec{r}'; \omega) \phi^{\text{SCF}}(\vec{r}', \omega) d\vec{r}'. \end{aligned} \quad (25)$$

Note that all induced quantities and hence  $\phi^{\text{SCF}}(\vec{r}, \omega)$  are frequency-dependent complex quantities proportional to the magnitude of the external electric field  $\mathcal{E}_0$ . The density will in general oscillate out of phase with the external field. Equations (22), (23), and (25) are solved simultaneously and the polarizability and total photoabsorption cross section are calculated using Eqs. (6) and (9), respectively.

In this theory, the kernel function  $K(\vec{r}, \vec{r}')$  is static, and all the time dependence of the induced fields is carried through the density  $\delta n(\vec{r}, \omega)$ .<sup>32</sup> In a more refined theory,  $K(\vec{r}, \vec{r}')$  would carry additional time dependence. It should be clear that our local-field correction only models those correlation effects which produce a polarization of the system.<sup>33</sup> The processes which lead to two-electron excitation, as mentioned in the Introduction, are beyond the scope of the present calculation.

To see the meaning of the local field more clearly, consider the following expression obtained from Eqs. (5), (6), (9), and (12):

$$\begin{aligned} \sigma(\omega) &= -\frac{16\pi\omega}{c\mathcal{E}_0^2} \text{Im} \int \phi^{\text{ext}}(\vec{r}, \omega) \chi_0(\vec{r}, \vec{r}'; \omega) \\ &\quad \times \phi^{\text{SCF}}(\vec{r}', \omega) d\vec{r} d\vec{r}'. \end{aligned} \quad (26)$$

Expanding the imaginary part as  $\text{Im}A = (A - A^*)/2i$  and using the SCF integral equation,

$$\begin{aligned} \phi^{\text{SCF}}(\vec{r}, \omega) &= \phi^{\text{ext}}(\vec{r}, \omega) \\ &\quad + \int K(\vec{r}, \vec{r}') \chi_0(\vec{r}', \vec{r}''; \omega) \\ &\quad \times \phi^{\text{SCF}}(\vec{r}'', \omega) d\vec{r}' d\vec{r}'', \end{aligned} \quad (27)$$

obtained from Eqs. (24) and (25), we readily obtain

$$\begin{aligned} \sigma(\omega) &= -\frac{16\pi\omega}{c\mathcal{E}_0^2} \int \phi^{*\text{SCF}}(\vec{r}, \omega) \text{Im} \chi_0(\vec{r}, \vec{r}'; \omega) \\ &\quad \times \phi^{\text{SCF}}(\vec{r}', \omega) d\vec{r} d\vec{r}'. \end{aligned} \quad (28)$$

Finally, writing out  $\chi_0(\vec{r}, \vec{r}'; \omega)$  explicitly, we find

$$\sigma(\omega) = 4\pi^2 \alpha \hbar \omega \sum_{i,j} f_i(1-f_j) |\langle j | \phi_{\omega}^{\text{SCF}}(r) Y_1^0(\hat{r}) | i \rangle|^2 \times \delta(\hbar\omega - \epsilon_j + \epsilon_i), \quad (29)$$

where

$$\phi_{\omega}^{\text{SCF}}(\vec{r}, \omega) = -\frac{1}{2} e \mathcal{E} \phi_{\omega}^{\text{SCF}}(r) Y_1^0(\hat{r}).$$

The dependence of  $\phi_{\omega}^{\text{SCF}}(\vec{r}, \omega)$  on the spherical harmonic  $Y_1^0(\hat{r})$  reflects the symmetry of the external field and implies that the usual dipole selection rules remain valid. Equation (29) should be compared with Eq. (13); the two are identical save for the replacement of the *external* field by the *local* field.

It is useful to compare the structure of our calculation to that of the RPAE.<sup>34</sup> They are in fact identical, with the Hartree-Fock single-particle orbitals, energies and electron-electron matrix elements replaced by LDA orbitals, energies, and linearized potentials, respectively. The important difference, however, is not one of structure but of computational simplicity. The local nature of the atomic potential permits an exact evaluation of the independent-particle susceptibility, Eq. (21), at least within the context of the model. We discuss this aspect more fully in the following section.

### III. DETAILS OF THE CALCULATION

#### A. $\chi_0(\vec{r}, \vec{r}'; \omega)$ and the atomic Green's function

The calculation of the self-consistent field polarizability requires a solution of the integral equation (25) and hence evaluation of the independent-particle susceptibility  $\chi_0(\vec{r}, \vec{r}'; \omega)$  given by Eq. (21). Note that this expression involves an explicit sum over the complete spectrum of the LDA effective single-particle potential  $V_{\text{eff}}(\vec{r})$ . That is, we require not only the occupied orbitals found simultaneously with  $V_{\text{eff}}(\vec{r})$ , but all unoccupied bound states and continuum orbitals as well. Previous investigators have typically approximated this infinite summation by various discretization schemes.<sup>35</sup> We shall circumvent this problem by use of the Green's function associated with the LDA Schrödinger-type equation. This Green's function satisfies the differential equation,

$$[E + \nabla^2 - V_{\text{eff}}(\vec{r})]G(\vec{r}, \vec{r}'; E) = \delta(\vec{r} - \vec{r}'), \quad (30)$$

where  $E$  is a parameter. We measure energies and lengths in rydberg and Bohr radii, respectively;  $G(\vec{r}, \vec{r}'; E)$  possesses an eigenfunction expansion,

$$G(\vec{r}, \vec{r}'; E) = \sum_m \frac{\varphi_m(\vec{r}) \varphi_m^*(\vec{r}')}{E - \epsilon_m \pm i\delta} \quad (31)$$

and satisfies the symmetry relation,

$$G(\vec{r}, \vec{r}'; E) = G^*(\vec{r}', \vec{r}; E). \quad (32)$$

The sign of the imaginary part in Eq. (31) is determined by the boundary conditions applied to the solution of Eq. (30). We use the Green's functions to rewrite<sup>36</sup> the expression for the susceptibility, Eq. (21), as

$$\begin{aligned} \chi_0(\vec{r}, \vec{r}'; \omega) &= \sum_{i \text{ OCC}} \varphi_i^*(\vec{r}) \varphi_i(\vec{r}') \sum_j \frac{\varphi_j(\vec{r}) \varphi_j^*(\vec{r}')}{\epsilon_i + \hbar\omega - \epsilon_j + i\delta} \\ &+ \sum_{i \text{ OCC}} \varphi_i(\vec{r}) \varphi_i^*(\vec{r}') \sum_j \frac{\varphi_j^*(\vec{r}) \varphi_j(\vec{r}')}{\epsilon_i - \hbar\omega - \epsilon_j + i\delta}, \quad (33) \end{aligned}$$

$$\begin{aligned} \chi_0(\vec{r}, \vec{r}'; \omega) &= \sum_{i \text{ OCC}} \varphi_i^*(\vec{r}) \varphi_i(\vec{r}') G(\vec{r}, \vec{r}'; \epsilon_i + \hbar\omega) \\ &+ \sum_{i \text{ OCC}} \varphi_i(\vec{r}) \varphi_i^*(\vec{r}') G^*(\vec{r}, \vec{r}'; \epsilon_i - \hbar\omega). \quad (34) \end{aligned}$$

Hence, we reduce the need for explicit wave functions to those already obtained by solution of Eqs. (14)–(16).

All that remains is an explicit construction of the Green's function.<sup>37</sup> Since the atomic system is rotationally invariant,

$$G(\vec{r}, \vec{r}'; E) = \sum_L Y_L^*(\hat{r}) G_L(r, r'; E) Y_L(\hat{r}'), \quad (35)$$

where  $L$  is a compact notation for the angular-momentum quantum numbers  $l$  and  $m$ . Equation (30) may then be written,

$$\left( E + \frac{1}{r^2} \frac{\partial}{\partial r} r^2 \frac{\partial}{\partial r} - \frac{l(l+1)}{r^2} - V_{\text{eff}}(r) \right) G_L(r, r'; E) = \frac{\delta(r - r')}{r^2}. \quad (36)$$

Let  $j_l(r|E)$  be the solution to the homogeneous version of Eq. (36) which satisfies the proper boundary condition at  $r=0$ , i.e., is regular at the origin. Similarly, let  $h_l(r|E)$  be the homogeneous solution which satisfies the boundary conditions as  $r \rightarrow \infty$ . The sign of the imaginary infinitesimal in Eq. (33) means that  $h_l(r|E)$  must behave asymptotically as an outgoing wave. Finally, the Green's function is constructed as

$$G_L(r, r'; E) = \frac{j_l(r_{<}|E) h_l(r_{>}|E)}{W[j_l, h_l]}, \quad (37)$$

where  $r_{<}$  ( $r_{>}$ ) refers to the smaller (larger) in magnitude of  $r$  and  $r'$ . The Wronskian  $W[j, h]$  is defined as

$$W[j, h] = r^2 [j(r)h'(r) - j'(r)h(r)]_{r=a}, \quad (38)$$

and is independent of  $a$ . In practice, the auxiliary functions  $j_i(r|E)$  and  $h_i(r|E)$  are found by numerical integration of the homogeneous equation using the Numerov method.<sup>38</sup> The independent-particle susceptibility is then simply evaluated using Eq. (34).

We solve the integral equation (25) by iteration using a relaxation method<sup>39</sup> and the Aitken procedure<sup>40</sup> to accelerate convergence. Note that if the result of the first iteration  $\delta n_0(\vec{r}, \omega)$  is inserted into Eq. (6) we obtain the independent particle approximation to  $\alpha(\omega)$ . Generally, upon convergence, we calculate the SCF approximation to  $\alpha(\omega)$  from Eq. (6) and the total photoabsorption using Eq. (9). We also directly obtain the local potential function  $\phi_\omega^{\text{SCF}}(r)$ .

#### B. Partial cross sections

$\phi_\omega^{\text{SCF}}(r)$  is used directly in Eq. (29) to compute partial cross sections. For absorption by a state with quantum numbers  $(nl)$  we write the initial state as

$$\psi_i(\vec{r}) = \frac{u_{ni}(r)}{r} Y_L(\hat{r}), \quad (39)$$

and the final state with wavevector  $\vec{K}$  and energy  $\epsilon$  as

$$\psi_f(\vec{r}) = 4\pi \sum_{L'} A_{i,L'} r^L P_{\epsilon L'}(r) Y_{L'}^*(\hat{K}) Y_L(\hat{r}). \quad (40)$$

$u_{ni}(r)$  is a bound eigenfunction of the LDA equation

$$-\frac{d^2\psi}{dr^2} + \left( \frac{l(l+1)}{r^2} + V_{\text{eff}}(r) \right) \psi = \epsilon\psi, \quad (41)$$

and  $P_{\epsilon l}(r)$  a continuum solution, regular at the origin. The complex coefficients  $A_i$  are found by requiring  $\psi_f(\vec{r})$  to behave asymptotically as an incident plane wave plus an incoming spherical wave.<sup>41</sup> With these conventions, the partial cross section becomes

$$\begin{aligned} \sigma_{ni}(\omega) &= 2(2l+1)\alpha(\hbar\omega)\sqrt{\epsilon} a_B^2 \\ &\times \sum_{L'} |A_{i,L'}|^2 |\langle l100 | l'0 \rangle|^2 \\ &\times \left| \int P_{\epsilon L'}(r) \phi_\omega^{\text{SCF}}(r) u_{ni}(r) dr \right|^2, \end{aligned} \quad (42)$$

where  $\langle l100 | l'0 \rangle$  is a Clebsch-Gordan coefficient. Notice that the real and imaginary parts of the local field contribute to the cross section without interference; that is,

$$\begin{aligned} \left| \int P_{\epsilon l} \phi_\omega^{\text{SCF}} u_{ni} dr \right|^2 &= \left| \int P_{\epsilon l} \text{Re} \phi_\omega^{\text{SCF}} u_{ni} dr \right|^2 \\ &+ \left| \int P_{\epsilon l} \text{Im} \phi_\omega^{\text{SCF}} u_{ni} dr \right|^2. \end{aligned} \quad (43)$$

We apply our formalism to the calculation of the static polarizability, total, and partial cross sections of the rare-gas atoms in the next section.

## IV. RESULTS AND DISCUSSION

### A. Static polarizability

As we have mentioned, there is no formal justification for the use of the density functional methods to describe anything other than ground-state properties. Indeed, a proper discussion of the action of the time-dependent Hamiltonian  $\mathcal{H}'$  of Sec. II requires a generalization of the original formalism. Unfortunately, very little progress has been made in this direction.<sup>42</sup> However, within the present discussion, there exists a case where the standard density-functional formalism should be exact in principle. Recall that the static polarizability is a ground-state property of an atom in the presence of a uniform electric field. If the exact functional  $E_{\text{xc}}[n]$  were known, our procedure would be exact.

Our computation of  $\alpha(0)$  provides a test of the local density approximation. In Table I we present our results for the static polarizability of the rare gas atoms: neon, argon, krypton, and xenon. Equation (12) shows that the accuracy of this calculation is mirrored by the accuracy of a total energy calculation. In fact, the LDA provides a very good representation of the total ground-state energy of many-electron systems.<sup>44</sup> The essential point is that the exchange-correlation energy is given by the interaction energy of one electron with the spherical part of the exchange-correlation hole charge. Therefore, the total energy is insensitive to the nonspherical part of the true hole and the LDA, which predicts a completely spherical hole of the correct volume, provides an accurate description.

The results in Table I show that the SCF static polarizability is always smaller than the independent-particle value; the atom appears less polarizable when electron correlations are

TABLE I. Static polarizabilities of the rare-gas atoms.  $\alpha_0$  is the result of an independent-particle calculation.  $\alpha^{\text{SCF}}$  is the self-consistent field value. Experimental values from Ref. 43.

	Static polarizability ( $\text{\AA}^3$ )		
	$\alpha_0$	$\alpha^{\text{SCF}}$	$\alpha_{\text{EXPT}}$
Neon	0.50	0.43	0.40 ± 0.01
Argon	2.60	1.74	1.64 ± 0.01
Krypton	4.11	2.60	2.48 ± 0.01
Xenon	6.89	4.12	4.04 ± 0.02

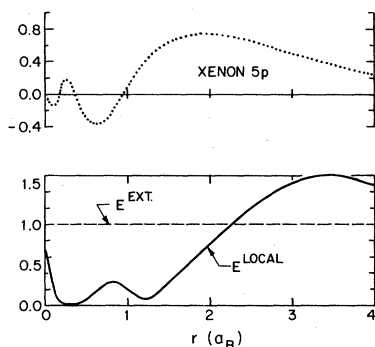


FIG. 1. Top panel: Normalized Xe 5p radial wave function. Bottom panel: External (dashed line) and local (solid line) electric field along the  $z$  axis for xenon at zero frequency. Field is measured in units of  $\frac{1}{2}\mathcal{E}_0$ . Positive values correspond to an electric field vector in the  $+\hat{z}$  direction.

switched on. We consider the xenon case in detail. In Fig. 1, the top panel shows the radial part of the outermost 5p orbital. In the decomposition of  $\alpha(0)$  implied by Eq. (34), this shell yields 80% of the total polarizability of xenon. The bottom panel shows the external electric field as a dashed line and the effective local electric field along the  $z$  axis as a solid line; i.e.,  $\vec{E}^{\text{local}}(z) = -(d/dr)\phi_{\omega}^{\text{SCF}}(r)\hat{z}$  with  $\omega=0$ . We emphasize that this is not the field that would be experienced by a test charge, due to the presence of the exchange-correlation potential in  $\phi_{\omega}^{\text{SCF}}(r)$ . At short distances, the magnitude of the local field is nearly zero. However, the external field is effectively antiscreened at large distances from the nucleus. This dielectric screening by the atomic electrons ultimately leads to a smaller induced moment.

We can understand this phenomenon in more detail as follows. In response to the external field, the electrons move to produce a net charge surplus on one side of the atom and a deficit on the other. The resulting induced field is represented by the equipotential plot in the top panel of Fig. 2. Very qualitatively, this field is similar to that which would be produced by two point charges on the  $\pm z$  axis, of equal magnitude and opposite sign, each at a distance from the origin coinciding with the final maximum of the Xe 5p orbital. The effective induced electric field has components which interfere either constructively or destructively with the external field depending upon the position in the atom. When the induced field is superposed with the external field we obtain the equipotential pattern shown in the bottom panel of Fig. 2. The screening effects become evident upon comparison with the external field equipotentials shown as dashed lines.

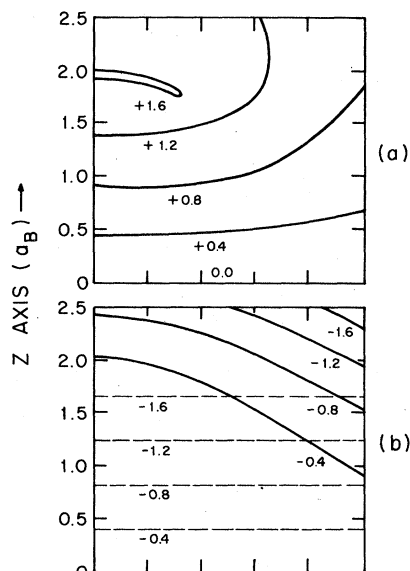


FIG. 2. Equipotential plots for xenon at zero frequency. The potentials have axial symmetry around the  $z$  axis and change sign upon reflection in the plane,  $z=0$ . Potential values are in units of  $\frac{1}{2}\mathcal{E}_0$ . Top panel: induced potential only. Bottom panel: induced potential plus external potential (solid lines), external potential only (dashed lines).

It is worth noting the effect of a slightly different  $V_{\text{eff}}(\vec{r})$  on this calculation. If the LDA potential is augmented by a Latter-type Coulomb tail,<sup>45</sup> the agreement with experiment is worsened by almost 50% in all the cases we have studied. This new potential is continuous, but suffers a sharp break when the LDA potential reaches the value  $-2/r$ . We presume that this change is sufficient to alter the volume of the exchange-correlation hole considerably. In any case, the results in the LDA are encouraging enough to proceed to nonzero frequency.

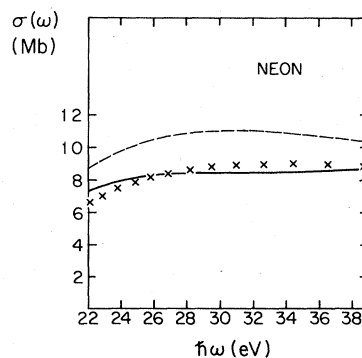


FIG. 3. Total photoabsorption cross section of neon versus photon energy in the vicinity of the 2p threshold; SCF calculation (solid line), independent-particle calculation (dashed line), data (crosses) from Ref. 46.

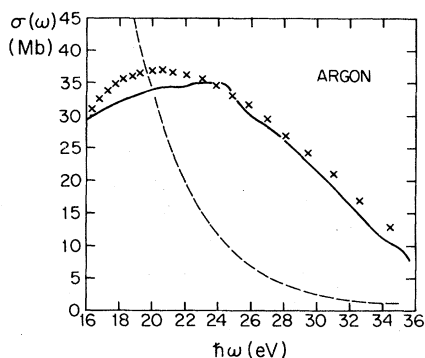


FIG. 4. Total photoabsorption cross section of argon versus photon energy in the vicinity of the  $3p$  threshold; SCF calculation (solid line), independent-particle calculation (dashed line), data (crosses) from Ref. 46.

#### B. Total photoabsorption cross section

The total photoabsorption cross sections for the four rare gases under discussion appear in Figs. 3–6. The solid lines refer to the SCF calculation and the crosses indicate the data. The independent particle cross sections are shown as dashed curves. In each case, the photon energy range displayed extends about 1 Ry above the first ionization threshold of the outermost  $p$  shell. In addition, Fig. 7 shows the total photoabsorption cross section for xenon on a different energy scale near the  $4d$ -shell threshold. The agreement with experiment is quite satisfactory and is comparable to that of other workers.<sup>49</sup> We wish to point out three aspects of these calculated cross sections.

First, our calculations do not show the characteristic autoionization resonances seen in high-precision measurements.<sup>50</sup> In principle, our

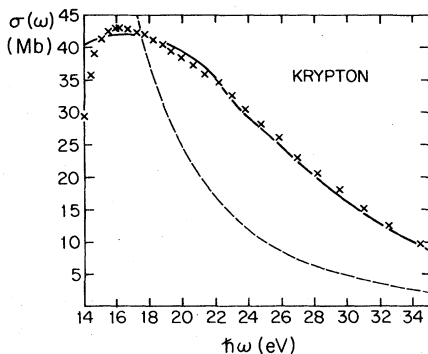


FIG. 5. Total photoabsorption cross section of krypton versus photon energy in the vicinity of the  $4p$  threshold; SCF calculation (solid line), independent-particle calculation (dashed line), data (crosses) from Ref. 46.

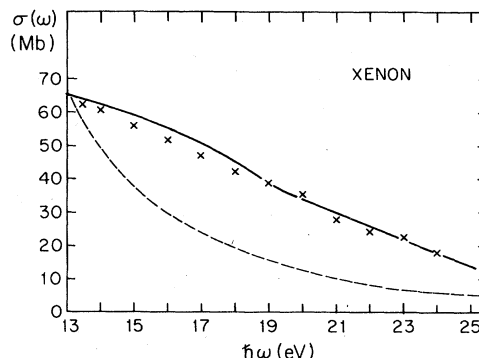


FIG. 6. Total photoabsorption cross section of xenon versus photon energy in the vicinity of the  $5p$  threshold; SCF calculation (solid line), independent-particle calculation (dashed line), data (crosses) from Ref. 47.

method is capable of describing this channel-mixing phenomenon. In practice, the resonances do not appear because the potential  $V_{\text{eff}}(\vec{r})$  does not support the high-lying bound (rydberg) states essential to the process. The failure here is due to the LDA which yields an effective potential which goes asymptotically to zero like the density, i.e., exponentially, rather than like  $-2/r$ . As in the static case, a Latter correction worsens the results. Other workers' systematic attempts to rectify this flaw in the LDA have led to an orbital dependent potential<sup>51</sup> or are sufficiently complex<sup>52</sup> to greatly diminish the computational simplicity of our method. The analog of the  $V^{N-1}$  potential<sup>53</sup> is unacceptable here since occupied and unoccupied orbitals must be determined from the same potential.

Second, the onset of continuous absorption for each atomic shell is given, in the theory, by the corresponding single-particle energy eigenvalue.

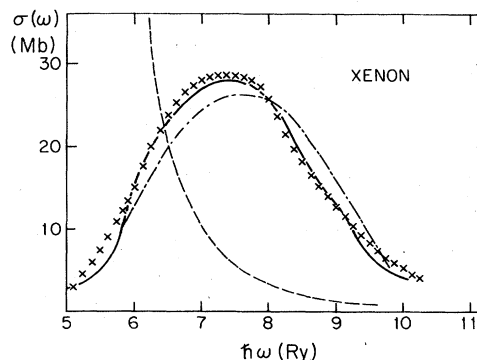


FIG. 7. Total photoabsorption cross section of xenon versus photon energy in the vicinity of the  $4d$  threshold. Note change in energy scale from Fig. 6; SCF calculation (solid line), independent-particle calculation (dashed line), SCF calculation with  $\delta V_{xc} = 0$  (dashed-dot line), data (crosses) from Ref. 48.

This is seen clearly in Eq. (29). Therefore, the calculated cross-section curves typically begin several volts lower in photon energy than the observed thresholds. For the situations shown in Figs. 3–6 this means that part of the continuous oscillator strength in the calculation lies in the discrete part of the true spectrum. Nonetheless, in the region of true physical absorption, the results are quite reasonable. We stress that our curves have not been shifted on the energy axis. This is particularly interesting in light of the sum rule, Eq.(11), and the good results for the static polarizability. The implication is that the contribution to the sum rule made by bound-to-bound transitions in the real atom is provided by the “unphysical” part of the continuous absorption distribution in our calculation.

Lastly, we consider the importance of the induced exchange–correlation potential, Eq. (23). In Fig. (7), the dashed-dot curve is the result of an SCF calculation with  $\delta V_{xc}(\vec{r})=0$ . The difference between this curve and the full calculation is at most about 10%. Nonetheless, the inclusion of this effect clearly brings the calculation into better accord with experiment. We conclude that the electron correlation effects built into the LDA ground state are sufficient to account for most of the polarization phenomena when only an induced Coulomb potential (RPA-type) calculation is performed.

We now interpret our results for the total photoabsorption cross section in terms of the local field. Consider first the case of xenon as shown in Fig. 7. At these energies the absorption is dominated by transitions from the 4d shell. Indeed, the striking resonance in the independent particle cross section near threshold is due to coupling to an  $f$ -wave virtual bound state. The characteristic redistribution of spectral weight toward higher photon energy may be understood with reference to Eqs. (42) and (43). The matrix elements there depend upon the real and imaginary parts of  $\phi_{\omega}^{\text{SCF}}(r)$  which are shown in Fig. 8. The corresponding radial part of the external potential is shown as a dashed line at each energy. At 5.5 Ry, the external potential is strongly screened in the region of maximum wave function overlap, with a subsequent reduction in the cross section relative to its independent-particle value. By 7.5 Ry, the contribution from  $\text{Re}\phi_{\omega}^{\text{SCF}}(r)$  nearly equals that of the external field. The induced field oscillates  $90^\circ$  out of phase with the driving field so that  $\text{Im}\phi_{\omega}^{\text{SCF}}(r)$  dominates the matrix elements and enhances  $\sigma(\omega)$ . Finally, at 9.5 Ry,  $\text{Im}\phi_{\omega}^{\text{SCF}}(r)$  is small again and the antiscreening of the external potential now provides the enhancement mechanism. In a preliminary report

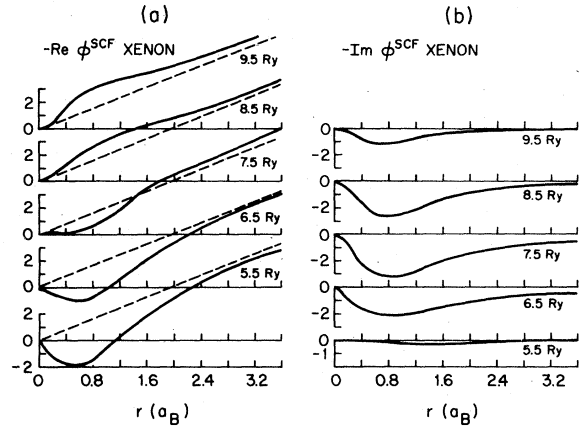


FIG. 8. (a) Real part of radial local potential,  $\text{Re}\phi_{\omega}^{\text{SCF}}(r)$  for xenon (solid lines), radial part of external potential (dashed lines). (b) Imaginary part of radial local potential,  $\text{Im}\phi_{\omega}^{\text{SCF}}(r)$  for xenon. All potentials measured in units of  $\frac{1}{2}\epsilon_0$ .

of this work<sup>54</sup> we have shown how the energy dependence of the phase of the induced field may be understood by analogy with the driven harmonic oscillator.

The magnitude and spatial variation of the dielectric screening effects in this case may be seen in Fig. 9. The top panel shows  $r\psi_{4d}(r)$  which is primarily responsible for the absorption in this energy range. The subsequent panels show the real part of the effective local electric field along the  $z$  axis,  $\vec{E}^{\text{loc}}(z) = -(d/dr)\text{Re}\phi_{\omega}^{\text{SCF}}(r)\hat{z}$ , as the photon energy passes through the self-con-

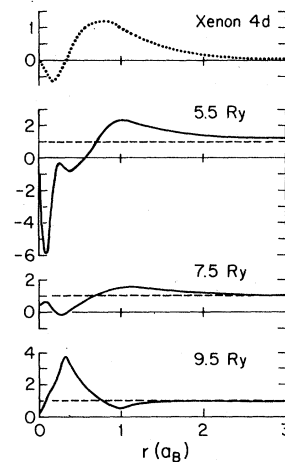


FIG. 9. Top panel: Normalized Xe 4d radial wave function. Subsequent panels: External (dashed lines) and local (solid lines) electric field along the  $z$  axis for xenon. Field is measured in units of  $\frac{1}{2}\epsilon_0$ . Positive values correspond to an electric field vector in the  $+\hat{z}$  direction.

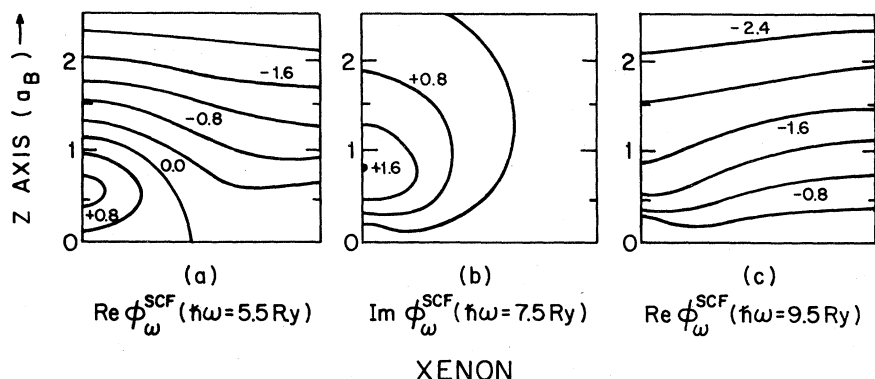


FIG. 10. Equipotential plots of real [(a) and (c)] and imaginary [(b) only] parts of local field for xenon. Display conventions as in Fig. 2. Adjacent equipotentials differ in potential by  $0.4(\frac{1}{2}\delta_0)$ .

sistently determined resonance position at about 7.5 Ry. The importance of the shell structure is illustrated by the point where the SCF field switches from screening to anti-screening behavior—in each case, it corresponds to the maximum in the  $4d$  radial wave function. Note also that the effective electric field actually changes sign in some regions of the atom at 5.5 and 7.5 Ry. Finally, we show in Fig. 10 the equipotentials of only the part of the SCF field (real or imaginary) which dominates the cross section at each energy. The dipolar field induced by the  $4d$  shell is obvious in  $\text{Im}\phi_{\omega}^{\text{SCF}}(r)$  at 7.5 Ry. Below resonance, at 5.5 Ry, this induced field is oscillating in phase with the external field. The situation is similar to the static case, except that here the induced field is strong enough near the nucleus to completely cancel the external field and to

actually change the direction of the electric field vector. Above resonance, the induced dipole turns  $180^\circ$  and antiscreens at short distances. We feel that each of the depicted representations of the local field is helpful toward gaining insight into the nature of the dielectric response.

The situation is quite similar in the other cases we have studied where the independent particle approximation fails to describe the cross-section data. Figure 11 shows the local potential  $\phi_{\omega}^{\text{SCF}}(r)$  associated with argon spanning the energy range of Fig. 4. Again, the curves reflect the characteristic screening which shifts the spectral weight away from the scattering resonance in the  $3p \rightarrow \epsilon d$  channel seen in the independent particle calculation. The portion of the induced potential associated with the distortion of the  $3p$  shell which oscillates  $90^\circ$  out of phase with the external potential attains its maximum value at about 25 eV, the position of the peak in the calculated cross section. The significant anti-screening of the potential at higher energy has an important in-

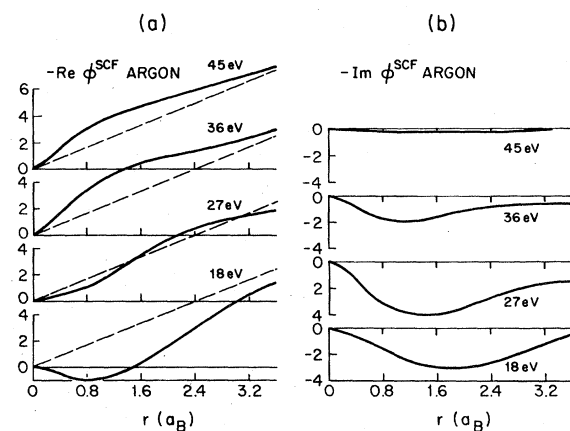


FIG. 11. (a) Real part of radial local potential,  $\text{Re}\phi_{\omega}^{\text{SCF}}(r)$  for argon (solid lines), radial part of external potential (dashed lines). (b) Imaginary part of radial local potential,  $\text{Im}\phi_{\omega}^{\text{SCF}}(r)$  for argon. All potentials measured in units of  $\frac{1}{2}\delta_0$ .

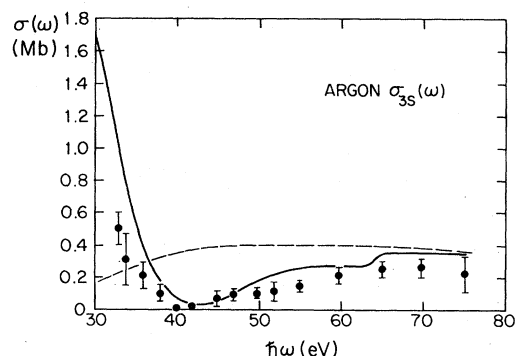


FIG. 12.  $3s$  partial photoabsorption cross section of argon; SCF calculation (solid line), independent particle calculation (dashed line), data from Ref. 55.

fluence on the emission from the 3s subshell of this atom.

### C. Partial cross sections

The partial photoabsorption cross section of the 3s shell of argon is shown in Fig. 12. The independent-particle calculation appears as a dashed line. We find good agreement with experiment for the position of the so-called Cooper minimum.<sup>56</sup> The source of this minimum is a zero in the matrix element,  $\langle \epsilon p | \text{Re} \phi_{\omega}^{\text{SCF}} | 3s \rangle$ . Furthermore, from the matrix element decomposition of Eq. (43) we find that the enormous enhancement of  $\sigma_{3s}(\omega)$  over the independent-particle value from the 3s threshold to the Cooper minimum is due almost entirely to  $\text{Im} \phi_{\omega}^{\text{SCF}}(r)$ , Fig. 11(b). That is, the field induced by the distortion of the 3p shell drives the emission from the 3s shell in this energy range. Amusia and co-workers<sup>57</sup> refer to this effect as intershell coupling. Beyond the minimum,  $\text{Im} \phi_{\omega}^{\text{SCF}}(r)$  falls to zero very rapidly, and  $\sigma_{3s}(\omega)$  is dominated by the real part of the field. The interpretation here is not quite so clear as in the xenon 4d case because canceling contributions to  $\langle \epsilon p | \text{Re} \phi_{\omega}^{\text{SCF}} | 3s \rangle$  actually suppress the cross section despite the antiscreening of the external potential. We mention in conclusion that we obtain very similar results for the 5s partial cross section of xenon.

### V. CONCLUSION

The work reported in this paper has demonstrated the successful application of the density

functional formalism, in the local-density approximation, to the calculation of the static polarizability, total photoabsorption cross section, and selected partial photoabsorption cross sections of the rare gas atoms. We have shown that polarization-type many-body effects may be conveniently incorporated into an effective local potential which replaces the dipole operator in the Golden Rule formulation of the cross section. In addition, the energy and position dependence of this complex local field have been used to gain insight into the screening properties of the atomic shells of these atoms. Finally, we have shown how a relatively simple numerical procedure can yield such results. The success of this demonstration has given us confidence that accurate cross sections for more complex systems may soon be obtained.

*Note added in proof.* After the completion of this work, we learned of a calculation of the static polarizability of the rare-gas atoms by M. J. Scott and E. Zaremba using techniques similar to our own. [Phys. Rev. A **21**, 12 (1980).]

### ACKNOWLEDGMENTS

We wish to thank Roy Marshall and the staff of the David Rittenhouse Laboratory Computation Center for their unflagging assistance through the course of this work. This work was supported in part by the National Science Foundation under Grants Nos. DMR 77-23420 and DMR 76-80994.

<sup>1</sup>See for example, H. Ehrenreich and M. H. Cohen, Phys. Rev. **115**, 786 (1959), and references therein.  
<sup>2</sup>W. Brandt and S. Lundqvist, Ark. Fys. **28**, 399 (1965).  
<sup>3</sup>See H. Ehrenreich and M. H. Cohen (Ref. 1) and M. Nakayama, Kyusyu University report (unpublished) for a viewpoint similar to that taken in this paper.  
<sup>4</sup>D. Pines and P. Nozieres, *The Theory of Quantum Liquids* (Benjamin, New York, 1966), Vol. 1, Chap. 4.  
<sup>5</sup>L. Hedin and S. Lundqvist in *Solid State Physics*, edited by F. Seitz and D. Turnbull (Academic, New York, 1969), Vol. 23.  
<sup>6</sup>O. Sinanoglu and K. Brueckner, *Three Approaches to Electron Correlations in Atoms* (Yale University Press, New Haven, 1970).  
<sup>7</sup>O. Gunnarsson and B. I. Lundqvist, Phys. Rev. B **13**, 4274 (1976).  
<sup>8</sup>O. Gunnarsson and B. I. Lundqvist, Phys. Rev. B **13**, 4274 (1976).  
<sup>9</sup>See O. Sinanoglu and K. Brueckner (Ref. 6).  
<sup>10</sup>D. M. P. Holland, K. Codling, J. B. West, and G. V. Marr, J. Phys. B **12**, 2465 (1979).  
<sup>11</sup>M. Y. Adam, F. Willeumier, S. Krummacher,

N. Sander, V. Schmidt, and W. Melhorn, J. Electron Spectros. **15**, 211 (1979).

<sup>12</sup>U. Fano and J. W. Cooper, Rev. Mod. Phys. **40**, 441 (1968).  
<sup>13</sup>P. L. Altick and A. E. Glassgold, Phys. Rev. **133**, A632 (1964).  
<sup>14</sup>M. Ya. Amusia and N. A. Cherepkov, Case Stud. At. Phys. **5**, 47 (1975).  
<sup>15</sup>G. Wendin, J. Phys. B **6**, 42 (1973).  
<sup>16</sup>H. P. Kelly, Comput. Phys. Commun. **17**, 99 (1979).  
<sup>17</sup>T. N. Chang and U. Fano, Phys. Rev. A **13**, 263 (1976).  
<sup>18</sup>P. G. Burke and K. T. Taylor, J. Phys. B **8**, 2620 (1975).  
<sup>19</sup>See for example, A. L. Fetter and J. D. Walecka, *Quantum Theory of Many-Body Systems* (McGraw-Hill, New York, 1971), Sec. 13.  
<sup>20</sup>See U. Fano and J. W. Cooper (Ref. 12), Sec. 2.5.  
<sup>21</sup>See for example, A. Dalgarno, Adv. Phys. **11**, 281 (1962).  
<sup>22</sup>S. T. Manson and J. W. Cooper, Phys. Rev. **165**, 126 (1968).  
<sup>23</sup>F. Combet-Farnoux, J. Phys. **30**, 521 (1968).

- <sup>24</sup>D. J. Kennedy and S. T. Manson, Phys. Rev. A 5, 227 (1972).
- <sup>25</sup>See M. Ya. Amusia and N. A. Cherepkov (Ref. 14); G. Wendin (Ref. 15); H. P. Kelly (Ref. 16); T. N. Chang and U. Fano (Ref. 17); P. G. Burke and K. T. Taylor (Ref. 18).
- <sup>26</sup>P. Hohenberg and W. Kohn, Phys. Rev. 136, B864 (1964); W. Kohn and L. Sham, *ibid.* 140, A1133 (1965).
- <sup>27</sup>W. Kohn and L. Sham, Phys. Rev. 140, A1133 (1965); see also O. Gunnarsson and B. I. Lundqvist (Ref. 7).
- <sup>28</sup>O. Gunnarsson in *Electrons in Disordered Metals and At Metal Surfaces*, NATO Advanced Study Institute, edited by P. Phariseau and B. L. Gyorffy (Plenum, New York, 1979), Vol. 42.
- <sup>29</sup>This is by now a commonly made assumption. For an example in atomic calculations see G. W. Bryant and G. D. Mahan, Phys. Rev. B 17, 1744 (1978).
- <sup>30</sup>See H. Ehrenreich and M. H. Cohen (Ref. 1) and N. Wiser, Phys. Rev. 129, 62 (1963) for a useful discussion of the local-field concept.
- <sup>31</sup>T. Schneider, Physica 52, 481 (1971); L. Hedin and B. I. Lundqvist, J. Phys. C 4, 2064 (1971).
- <sup>32</sup>T. Schneider, Physica 52, 481 (1971); L. Hedin and B. I. Lundqvist, J. Phys. C 4, 2064 (1971).
- <sup>33</sup>See W. Brandt and S. Lundqvist (Ref. 2).
- <sup>34</sup>See M. Ya. Amusia and N. A. Cherepkov (Ref. 14); G. Wendin (Ref. 15).
- <sup>35</sup>See M. Ya. Amusia and N. A. Cherepkov (Ref. 14); G. Wendin (Ref. 15).
- <sup>36</sup>This technique has been used previously. See for example, P. Fiebelman, Phys. Rev. B 12, 1319 (1975), where a local-field calculation for a metal surface in the LDA is performed.
- <sup>37</sup>See for example, Jon Mathews and R. L. Walker, *Mathematical Methods of Physics* (Benjamin, New York, 1965), Sec. 9.4.
- <sup>38</sup>D. R. Hartree, *The Calculation of Atomic Structures* (Wiley, New York, 1957), Sec. 4.5.
- <sup>39</sup>D. R. Hartree, *The Calculation of Atomic Structures* (Wiley, New York, 1957), Sec. 5.3.3.
- <sup>40</sup>See for example, Forman S. Acton, *Numerical Methods That Work* (Harper and Row, New York, 1970), p. 216.
- <sup>41</sup>G. Breit and H. A. Bethe, Phys. Rev. 93, 888 (1954).
- <sup>42</sup>See, however, V. Peuckert, J. Phys. C 11, 4945 (1978), and references therein.
- <sup>43</sup>T. M. Miller and B. Bederson in *Advances in Atomic and Molecular Physics*, edited by D. R. Bates and B. Bederson (Academic, New York, 1977), Vol. 13.
- <sup>44</sup>See O. Gunnarsson and B. I. Lundqvist (Ref. 7).
- <sup>45</sup>R. Latter, Phys. Rev. 81, 385 (1955).
- <sup>46</sup>G. V. Marr and J. B. West, At. Data Nucl. Data Tables 18, 497 (1976).
- <sup>47</sup>R. D. Hudson and L. J. Kieffer, At. Data 2, 205 (1970).
- <sup>48</sup>R. Haensel, G. Keitel, P. Schrieber, and C. Kunz, Phys. Rev. 188, 1375 (1969).
- <sup>49</sup>See M. Ya. Amusia and N. A. Cherepkov (Ref. 14).
- <sup>50</sup>R. P. Madden, D. L. Ederer, and K. Codling, Phys. Rev. 177, 136 (1969).
- <sup>51</sup>J. P. Perdew, Chem. Phys. Lett. 64, 127 (1969).
- <sup>52</sup>O. Gunnarsson and R. O. Jones, Phys. Scr. (in press).
- <sup>53</sup>See H. P. Kelly (Ref. 16).
- <sup>54</sup>A. Zangwill and Paul Soven, J. Vac. Soc. (in press).
- <sup>55</sup>K. H. Tan and C. E. Brion, J. Electron Spectros. 13, 77 (1978).
- <sup>56</sup>See U. Fano and J. W. Cooper (Ref. 12).
- <sup>57</sup>M. Ya. Amusia, V. K. Ivanov, N. A. Cherepkov, and L. V. Chernysheva, Zh. Eksp. Teor. Fiz. 66, 1537 (1974) [Sov. Phys. JETP 39, 752 (1974)].